Special Issue Article

Journal of PeptideScience

Received: 30 September 2014 Revised: 9 December 2014 Accepted: 11 December 2014 Published online in Wiley Online Library

(wileyonlinelibrary.com) DOI 10.1002/psc.2740

An investigation into the origin of the biased agonism associated with the urotensin II receptor activation**

Diego Brancaccio,[a‡] Francesco Merlino,[a‡] Antonio Limatola,[a] Ali Munaim Yousif,[a] Isabel Gomez-Monterrey,[a] Pietro Campiglia,[b] Ettore Novellino,[a] Paolo Grieco[a,c] and Alfonso Carotenuto[a]*

The urotensin II receptor (UTR) has long been studied mainly for its involvement in the cardiovascular homeostasis both in health and disease state. Two endogenous ligands activate UTR, i.e. urotensin II (U-II) and urotensin II-related peptide (URP). Extensive expression of the two ligands uncovers the diversified pathophysiological effects mediated by the urotensinergic system such as cardiovascular disorders, smooth muscle cell proliferation, renal disease, diabetes, and tumour growth. As newly reported, U-II and URP have distinct effects on transcriptional activity, cell proliferation, and myocardial contractile activities supporting the idea that U-II and URP interact with UTR in a distinct manner (biased agonism). To shed light on the origin of the divergent activities of the two endogenous ligands, we performed a conformational study on URP by solution NMR in sodium dodecyl sulfate micelle solution and compared the obtained NMR structure of URP with that of *h*U-II previously determined. Finally, we undertook docking studies between URP, *h*U-II, and an UT receptor model. Copyright © 2015 European Peptide Society and John Wiley & Sons, Ltd.

Additional supporting information may be found in the online version of this article at the publisher's web site.

Keywords: urotensin-II; urotensin II-related peptide; therapeutic peptide; biased agonism; conformation by NMR; docking studies

Introduction

Among a series of regulatory neuropeptides isolated from urophysis of goby fish, urotensin II (U-II) was characterized as an important vasoactive cyclic peptide [1]. It has been postulated that this peptide hormone exerts wide range of pathophysiological actions not exclusively in the cardiovascular system. From the identification of U-II precursor in frog brain [2], it was demonstrated that DNA encoding for U-II existed in diverse species. Indeed, homologous peptides of U-II are expressed in non-mammalian and mammalian vertebrates, including humans [3–6]. The human U-II (*h*U-II) acts as the innate ligand of a G protein-coupled receptor, more recently known as UT receptor (UTR) [7]. In 2003, Sugo *et al.* [8] proved the existence of a paralogue of *h*U-II so called urotensin II-related peptide (URP). This peptide is structurally related to *h*U-II and displays elevated binding affinity for the human UTR in mammals. Despite of the highly variable N-terminus region sequence across species (Figure 1), every U-II and URP isopeptide shares the fully conserved cyclic C-terminal hexapeptide core sequence, c [Cys-Phe-Trp-Lys-Tyr-Cys], which is responsible of the biological activity [9]. The genes expressing *h*U-II and URP are mainly located in motoneurons of brainstem nuclei and ventral horn in the spinal cord [10–13]. *h*U-II and URP messenger RNAs have also been found in different peripheral tissues such as heart, thymus, pancreas, kidney, intestine, adrenal gland, prostate, and more [3,8,14]. As well as UTR is broadly distributed in the cardiovascular and central nervous system and in other peripheral organs and tissues, including kidneys, bladder, pancreas, and adrenal gland [15]. This extensive expression has resulted in the involvement of urotensinergic system in multiple pathophysiological effects interesting primarily cardiovascular conditions. Hence, modulation of urotensinergic system is therapeutically appealing in order to deal with different pathological disorders [16,17].

* *Correspondence to: Alfonso Carotenuto, Dipartimento di Farmacia., Università di Napoli 'Federico II', Via D. Montesano, 49, 80131 Naples, Italy. E-mail: alfonso.carotenuto@unina.it*

‡ *These authors equally contributed as co-first to the paper.*

** *Special issue of contributions presented at the 14th Naples Workshop on Bioactive Peptides "The renaissance era of peptides in drug discovery", June 12–14, 2014, Naples".*

a *Department of Pharmacy, University of Naples 'Federico II', I-80131, Naples, Italy*

b *Department of Pharmacy, University of Salerno, I-84084, Fisciano, Salerno, Italy*

c *CIRPEB: Centro Interuniversitario di Ricerca sui Peptidi Bioattivi University of Naples 'Federico II', DFM-Scarl, Institute of Biostructures and Bioimaging – CNR, 80134, Naples, Italy*

Abbreviations: *1D, 2D, and 3D, one-dimensional, two-dimensional, and three-dimensional; DCM, dichloromethane; DIEA, N,N-diisopropylethylamine; DMSO, dimethylsulfoxide; DQF-COSY, double quantum filtered correlated spectroscopy; HBTU, N,N,N',N'-tetramethyl-O-(1H-benzotriazol-1-yl)uroniumhexa-fluorophosphate; HOBt, 1-hydroxybenzotriazole; MD, molecular dynamics; NOESY, nuclear Overhauser enhancement spectroscopy; NOE, nuclear Overhauser effect; NMR, nuclear magnetic resonance; SDS, sodium dodecyl sulfate; SAR, structure activity relationship; TFA, trifluoroacetic acid; TOCSY, total correlated spectroscopy; Trt, triphenylmethyl; TSP, 3-(trimethylsilanyl)propionic acid; URP, urotensin II-related peptide; UTR, urotensin II receptor; h-UTR, human urotensin II receptor; U-II, urotensin II peptide; hU-II, human urotensin II peptide.*

Species	Sequence
	Urotensin II
Mouse	<Gln-His-Lys-Gln-His-Gly-Ala-Ala-Pro-Glu-Cys-Phe-Trp-Lys-Cys-Ile-OH
Rat	<Gln-His-Gly-Thr-Ala-Pro-Glu-Cys-Phe-Trp-Lys-Cys-Ile-OH
Chimpanzee	H-Glu-Thr-Pro-Asp-Cys-Phe-Trp-Lys-Cys-Val-OH
Human	H-Glu-Thr-Pro-Asp-Cys-Phe-Trp-Lys-Cys-Val-OH
	URP
Mouse	H-Ala-Cys-Phe-Trp-Lys-Cys-Val-OH
Rat	H-Ala-Cys-Phe-Trp-Lys-Cys-Val-OH
Chimpanzee	H-Ala-Cys-Phe-Trp-Lys-Cys-Val-OH
Human	H-Ala-Cys-Phe-Trp-Lys-Cys-Val-OH

Figure 1. Comparison of the primary structures of mammalian U-II and URP. Conserved amino acids in U-II and URP isoforms are coloured blue (intracyclic residues) and green (hydrophobic residue). Amino acids adjacent to the cyclic core are coloured red for U-II isoforms (acidic residues) or orange for URP isoforms (hydrophobic amino acid) to highlight their different physicochemical properties. <Gln represents pyroglutamic acid.

As recently reported, *h*U-II and URP can exert common as well as different effects on transcriptional activity, cell proliferation, and myocardial contractile activities supporting the idea that *h*U-II and URP interact with UTR in a distinct manner, i.e. by selecting a specific UT conformation (biased agonism) [18]. The concept of biased agonism has recently emerged from various studies, which have highlighted the notion that specific ligand-induced conformational changes can lead to particular signalling [19]. Biased agonism would require specific pockets/interactions within UT receptor, aimed to select distinct UTR conformations that can discriminate *h*U-II and URP biological activities. It has been postulated that a different conformation of the cyclic portion of these two peptides, β-turn in *h*U-II *versus* γ-turn in URP, would cause the selection of different UTR active states, ultimately triggering a slightly different subset of signalling pathways [18].

To investigate the origin of the divergent activities of the two endogenous ligands, we performed conformational studies on URP by solution NMR and compared the obtained NMR structure of URP with that of *h*U-II previously determined. Finally, we undertook docking studies between URP, *h*U-II, and a newly developed UT receptor model.

Materials and Methods

Peptide Synthesis

N^{α}-Fmoc-protected amino acids, HBTU, and HOBt were purchased from Inbios (Naples, Italy). Wang resin was purchased from Advanced ChemTech (Louisville, KY). Peptide synthesis solvents, reagents, as well as CH_3CN for HPLC were reagent grade and were acquired from commercial sources and used without further purification unless otherwise noted. The synthesis of URP was performed in a stepwise fashion via the solid-phase method. N^{α}-Fmoc-Val-OH was coupled to Wang resin in the presence of HBTU (3 equiv), HOBt (3 equiv), DIEA (6 equiv) and DMAP in catalytic amount, to facilitate ester formation, in DMF for 3 h at rt. The following protected amino acids were then added stepwise: N^{α}-Fmoc-Cys(Trt)-OH, N^{α}-Fmoc-Tyr(*t*Bu)-OH, N^{α}-Fmoc-Lys(N^{ε}-Boc)-OH, N^{α}-Fmoc-Trp(N^{in}-Boc)-OH, N^{α}-Fmoc-Phe-OH, N^{α}-Fmoc-Cys(Trt)-OH, and N^{α}-Fmoc-Ala-OH. Each coupling reaction was accomplished using a threefold excess of amino acid with HBTU and HOBt in the presence of DIEA (6 equiv).

The N^{α}-Fmoc protecting groups were removed by treating the protected peptide resin with a 25% solution of piperidine in DMF, (1 × 5 and 1 × 20 min). The peptide resin was washed three times with DMF and the subsequent coupling step was initiated in a stepwise manner. All reactions were performed under a N_2 atmosphere. The peptide resin was washed with DCM (3×), DMF (3×), and DCM (4×), and the deprotection protocol was repeated after each coupling step. The N-terminal Fmoc group was removed as described in the preceding text, and the peptide was released from the resin with TFA/Et_3SiH/H_2O (90 : 5 : 5) for 3 h. The resin was removed by filtration, and the crude peptide was recovered by precipitation with cold anhydrous ethyl ether to give a white powder that was purified by RP-HPLC on a semi-preparative C18-bonded silica column (Vydac 218TP1010, 1.0 × 25 cm) using a gradient of CH_3CN in 0.1% aqueous TFA (from 10 to 90% in 45 min) at a flow rate of 5.0 ml/min. The product was obtained by lyophilization of the appropriate fractions after removal of the CH_3CN by rotary evaporation. Analytical RP-HPLC indicated purity >98% and molecular weights were confirmed by ESI-MS analyses performed by API 2000 (Supporting Information, Table S1).

General Method of Oxidation and Cyclization

Peptide was oxidized by the syringe pump method previously reported [20]. The linear peptide (300–500 mg) was dissolved in 40 ml of 50% H_2O/25% acetonitrile/25% methanol, and nitrogen gas was passed through the solution for 20 min. Five millilitres of saturated ammonium acetate solution were added, and the pH was taken to 8.5 with NH_4OH. The peptide solution was then added at room temperature via syringe pump to a stirred oxidant solution. The oxidant solution was prepared as follows: 2 equiv of potassium ferricyanide were dissolved in 400 ml of H_2O/200 ml of acetonitrile/200 ml of methanol. To this solution was added 100 ml of saturated ammonium acetate, and the pH was then taken to 8.5 with NH_4OH. The peptide solution was added at such a rate that approximately 10 mg of peptide were delivered per hour per litre of the oxidant. After the addition of peptide was complete, the reaction mixture was stirred for an additional 5–6 h and then taken to pH 3.5 with glacial acetic acid. Amberlite IRA-68 (Cl – form) was added to remove the iron ions, and the solution stirred for 20 min and then filtered. The solution was concentrated using a rotary evaporator at 30°C and then lyophilized. The material thus obtained was dissolved in glacial acetic acid, filtered to remove inorganic salts, and relyophilized. The crude cyclic peptide was purified by preparative HPLC on the system described in the preceding texts, using a gradient of 100% buffer for 20 min, then 0–20% acetonitrile in 5 min, followed by 20–60% acetonitrile in 40 min, all at 40 ml/min. Again, the peptide eluted near 50% organic/50% buffer. The purity of the cyclic peptide was checked by analytical HPLC (C-18 column, Vydac 218TP104, 4,6 × 25 cm), using a Shimadzu SPD 10A vp with detection at 230 and 254 nm and by TLC in four solvent systems in silica gel with detection by

Journal of PeptideScience

UV light, iodine vapours, and ninhydrin. The analytical data of URP are given in the Supporting Information (Table S1).

Materials for NMR

99.9% ^2H_2O were obtained from Aldrich (Milwaukee, USA); 98% sodium dodecyl sulfate (SDS)-d_{25} was obtained from Cambridge Isotope Laboratories, Inc. (Andover, USA), [(2,2,3,3-tetradeuterio-3-(trimethylsilanyl)]propionic acid (TSP) from MSD Isotopes (Montreal, Canada).

NMR Spectroscopy

The samples for NMR spectroscopy were prepared by dissolving the appropriate amount of URP in 0.45 ml of ^1H_2O (pH 5.5), 0.05 ml of ^2H_2O to obtain a concentration 1–2 mM of peptide. For the sample in micelle solution, SDS-d_{25} was also added to a concentration of 200 mM. NMR spectra were recorded on a Varian INOVA 700 MHz spectrometer equipped with a z-gradient 5 mm triple-resonance probe head. Spectra in water solution and micelle were recorded at a temperature of 10 and 25°C, respectively. The spectra were calibrated relative to TSP (0.00 ppm) as internal standard. 1D NMR spectra were recorded in the Fourier mode with quadrature detection. The water signal was suppressed by gradient echo [21]. 2D DQF-COSY [22,23], TOCSY [24], and NOESY [25] spectra were recorded in the phase-sensitive mode using the method from USA [26]. Data block sizes were 2048 addresses in t_2 and 512 equidistant t_1 values. Before Fourier transformation, the time domain data matrices were multiplied by shifted $\sin^2$ functions in both dimensions. A mixing time of 70 ms was used for the TOCSY experiments. NOESY experiments were run with mixing times in the range of 150–300 ms. The qualitative and quantitative analyses of DQF-COSY, TOCSY, and NOESY spectra were obtained using the interactive program package XEASY [27]. $^3J_{HN\text{-}H\alpha}$ coupling constants were obtained from 1D ^{1}H NMR and 2D DQF-COSY spectra. The temperature coefficients of the amide proton chemical shifts were calculated from 1D ^{1}H NMR and 2D TOCSY experiments performed at different temperatures in the range 25–40°C by means of linear regression.

Structural Determinations

The NOE-based distance restraints were obtained from NOESY spectra collected with a mixing time of 200 ms. The NOE cross peaks were integrated with the XEASY program and were converted into upper distance bounds using the CALIBA program incorporated into the program package DYANA [28]. Cross peaks that were overlapped more than 50% were treated as weak restraints in the DYANA calculation. Only NOE-derived constraints (Supporting Information) were considered in the annealing procedures. An ensemble of 200 structures was generated with the simulated annealing of the program DYANA. An error-tolerant target function (tf-type = 3) was used to account for the peptide intrinsic flexibility. From the produced 200 conformations, 50 structures were chosen, whose interproton distances best fitted NOE derived distances and then refined through successive steps of restrained and unrestrained energy minimization using the Discover algorithm (Accelrys, San Diego, CA) and the consistent valence force field [29] as previously described [30]. The final structures were analysed using the InsightII program (Accelrys, San Diego, CA). Molecular graphics images of the complexes were produced using the UCSF Chimera package [31].

h-UTR Model and Docking

3D structure predictions of *h*-UTR were generated by I-TASSER server for protein structure and function prediction, which is based on a threading alignment algorithm [32–34]. Five models of *h*-UTR were obtained using I-TASSER servers. The best scored model (model 1, refer to Results Section) was used for docking studies.

The initial poses for the *h*-UTR–URP complex are generated by docking the lowest energy conformers of URP obtained by NMR to the *h*-UTR model using the program HADDOCK 2.0 [35,36]. For comparative purpose, also the best scored NMR structure of *h*U-II [30] was docked to the same *h*-UTR model. Only the distance between N^{ε} of Lys^8 and carboxyl oxygens of Asp130 on TM3 was used as a restraint (2.7 ± 1 Å) in the docking studies because the last residue is generally regarded as the ligand recognition site [37].

Considering the receptor, only the side chains of residues engaged in orthosteric ligand/GPCR binding in the complexes used as templates by I-TASSER (PDB IDs: 4n6h, 4dkl, 4buo; refer to Results Section) were considered flexible in the docking procedure (active residue: W116, L126, F127, D130, F131, M134, V184, M188, H208, L212, F274, W275, W277, Q278, Y305). Instead, all peptide's atoms were held frozen (passive residue).

Refinement of each pose was achieved by *in vacuo* energy minimization with the Discover algorithm using the steepest descent and conjugate gradient methods until a RMSD of 0.05 kcal/mol/Å was reached. The backbone atoms of the TM and IL domains of the *h*-UTR were held in their position; the ligand and extracellular loops (ELs) were free to relax. Molecular graphics images of the complexes were produced using the UCSF Chimera package [31].

Results

Chemistry

The peptide URP was synthesized by solid-phase strategy. The Fmoc/tBu orthogonal protecting groups were used, and the synthesis was accomplished in a manual reaction vessel [38] (Experimental Section). The crude peptide was purified by using a semi-preparative RP-HPLC equipped with C-18 bonded silica column (Vydac 218TP1010). The purified peptide was analysed by analytical RP-HPLC showing >98% purity. Exact molecular weight of the peptide was proved by mass spectrometry and amino acid analysis (Supporting Information, Table S1).

NMR Analysis

1D and 2D NMR spectra were collected in water and 200 mM aqueous solution of SDS for URP. Micelle solution was used because we have studied the NMR structure of *h*U-II and other UTR agonists [30,39,40] and antagonist [41] in this *medium*.

Complete ^{1}H NMR chemical shifts assignment was accomplished according to the Wüthrich procedure [42] via the analysis of DQF-COSY [22,23], TOCSY [24], and NOESY [25] spectra using the XEASY software package (Supporting Information, Tables S2 and S3) [27].

Considering the spectra in water solution, many NMR parameters indicate structural flexibility (Table S2). For example, H_α chemical shift values are all close ($\Delta\delta < 0.1$ ppm) to the corresponding ones in random coil peptides [43] apart that of Lys^8 (for easy comparison, peptide numbering of URP follows that of *h*U-II).

In contrast, NMR parameters derived from spectra acquired in SDS micelles are typical of a structured peptide (Table S3). Furthermore, such parameters indicated that URP structure is similar

to other UTR ligands previously studied by us, especially to its paralog *h*U-II. For comparison purpose, H_α chemical shifts of residues of *h*U-II constituting the cyclic moiety common to URP are also reported in Table S3. In particular, NOE contacts between H_α–NH_{i+2} of Trp^7 and Tyr^9 and between NH–NH_{i+1} of Lys^8 and Tyr^9 indicated the presence of a β-turn. The observation of slowly exchanging NH resonance of residue 9, and low value of the temperature coefficient for this proton ($-\Delta\delta/\Delta T < 3.0$ ppb/K) confirmed this result. A number of long-range NOEs including H_α–NH connectivities between residues 5, 11, and 10, 6 and a NH–NH connectivity between residues 6 and 9 supported the existence of a short stretch of antiparallel β-sheet involving residues 5–6 and 10–11. Also, large values of $^3J_{HN\text{-}H\alpha}$ coupling constants ($^3J_{HN\text{-}H\alpha} > 8.0$ Hz) for residues 5 and 9–11 confirm a β-sheet structure (Table S3). Overall data supported the existence of the β-hairpin structure in URP. Furthermore, many NOE interactions between Trp^7 with Lys^8 side chains implied that those side chains are close. Also, Tyr^9 side chain shows NOE contacts with Lys^8, while Phe^6 shows contacts with Val^{11}.

Constraints derived from NMR data were used as the input for a structure calculation by simulated annealing. Structure calculations using NMR data from URP spectra acquired in water gave not converging results (backbone RMSD > 2 Å for the 10 lowest energy conformers; data not shown). Differently, using the NMR constraints from SDS micelle solution (Table S4), an ensemble of well-defined structures could be obtained. In fact, the 10 lowest energy structures (Figure 2) showed a backbone RMSD of 0.34 Å and satisfied the NMR-derived constraints (violations smaller than 0.20 Å). As shown, URP folds into a type II′ β-hairpin structure along residues 5–10. Considering the side chain orientation, Phe^6, Trp^7, Lys^8, and Tyr^9 χ_1 angles showed a high preference for g^-, *trans*, g^+, and g^- rotamers, respectively. URP-obtained NMR structure is very similar to those of other UTR ligands previously found by us and, in particular, to that of *h*U-II (Figure 3).

h-UTR Model and Docking

3D models of *h*-UTR were generated based on the structure of other GPCR, using the I-TASSER server [32–34]. Five models of *h*-UTR were generated using I-TASSER server. I-TASSER output also contained top ranks of templates used for the structure prediction.

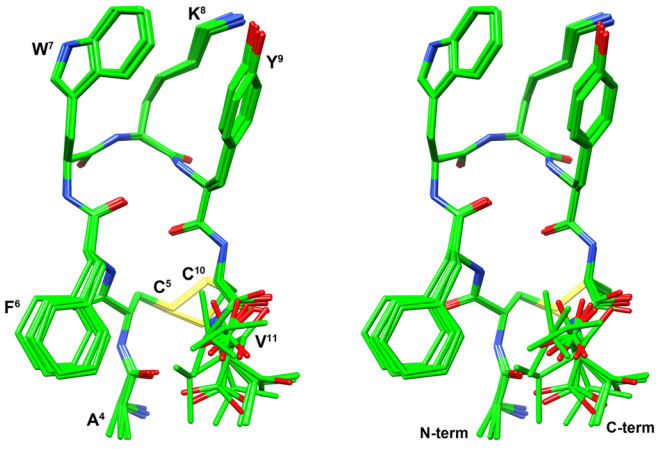

Figure 2. Stereoview of the superposition of the 10 lowest energy conformers of URP. Structures were superimposed using the backbone heavy atoms of residues 5–10. Heavy atoms are shown with different colours (carbon, green; nitrogen, blue; oxygen, red; sulfur, yellow). Hydrogen atoms are not shown for clarity.

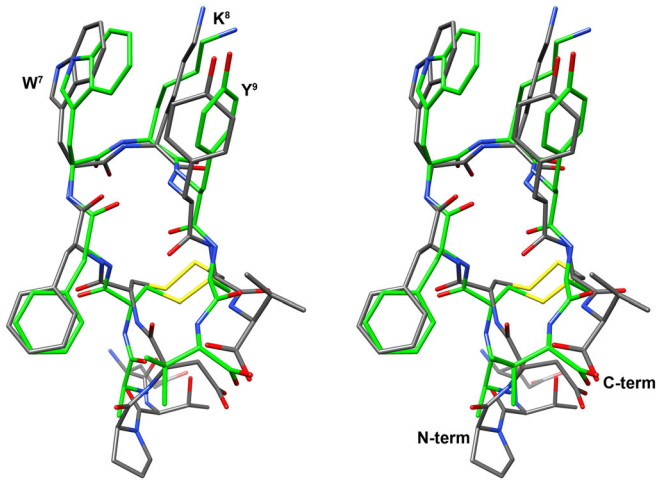

Figure 3. Stereoview of the superposition of the lowest energy conformer of URP (coulor code as in Figure 2) and *h*U-II (carbon atoms in grey). Structures were superimposed using the backbone heavy atoms of residues 5–10.

The top template used is the high-resolution crystal structure of human δ-opioid receptor (*h*-DOR, PDB ID: 4n6h) [44]. Other templates used for threading are the crystal structure of mouse μ-opioid receptor (*m*-MOR, PDB ID: 4dkl) [45] and the crystal structure of a neurotensin receptor 1 mutant (NTSR1, PDB ID: 4buo) [46]. The most important score in I-TASSER models is the confidence score (C-score), ranging from −5 to +2. The C-score is computed from the threading alignments for the estimated quality of the models. A C-score > −1.5 implies a model with a correct fold [34]. Model 1 of *h*-UTR (C-score = 1.56) with higher C-scores was chosen as the best model and was considered for the analyses. The model predictions were judged using the template modelling (TM) score and root mean-squared difference (rmsd). The TM score is a measure of the structural similarity between the model and the native structure. A TM score > +0.5 suggests a model with correct topology. The TM score of model 1 for *h*-UTR was 0.93 ± 0.06 Å. The expected RMSDs were 3.0 ± 2.2 Å. Additionally, to confirm the reliability of the model 1, the program PROCHECK [47] was employed. All amino acids in the α-helices were found in the favoured region of the right-handed α-helix in the Ramachandran plot. There were no cis peptide bonds, and there were no bump regions in the calculated *h*-UTR models. The results reveal that our 3D model for *h*-UTR is acceptable and of high quality. Worth to note, the selected model 1 maintain most of the molecular signatures that feature class A GPCR [48]. For example, in the selected model are present 24 out of the 24 inter-TM contacts of the consensus network found in the GPCR structures. A superposition of *h*-DOR crystal structure and *h*-UTR model 1 is shown in Figure S1 (Supporting Information).

Docking procedures using the program HADDOCK [35,36] clustered 198 structures in two clusters for both the complexes *h*-UTR/URP and *h*-UTR/*h*U-II. Statistics and energy terms are reported in Table 1. Best scored complexes of *h*-UTR/URP and *h*-UTR/*h*U-II are shown in Figures 4 and 5, respectively.

Discussion

U-II and URP could exert common as well as distinct actions on cell proliferation, transcriptional activity, and myocardial

Journal of PeptideScience

Table 1. Statistics and energy terms of the calculated complexes.

Complex	Cluster n.	H score[a]	Cluster size	RMSD[b]	VdW[c]	Eletr[d]	Desolv[e]
h-UTR/URP	1	−130.1 ± 2.6	191	0.5 ± 0.3	−56.6 ± 3.9	−150.9 ± 21.8	−49.3 ± 3.5
h-UTR/URP	2	−102.1 ± 2.5	7	0.8 ± 0.0	−50.7 ± 2.8	−166.3 ± 17.7	−28.4 ± 7.5
h-UTR/*h*U-II	1	−144.2 ± 2.5	193	1.3 ± 0.0	−56.2 ± 6.5	−230.2 ± 26.2	−48.5 ± 2.5
h-UTR/*h*U-II	2	−113.4 ± 13.2	5	1.1 ± 0.0	−56.6 ± 4.0	−210.2 ± 10.4	−24.8 ± 9.8

[a]HADDOCK score.
[b]RMSD from the overall lowest energy structure.
[c]Van der Waals energy.
[d]Electrostatic energy.
[e]Desolvation energy. All terms are given in Kcal/mol.

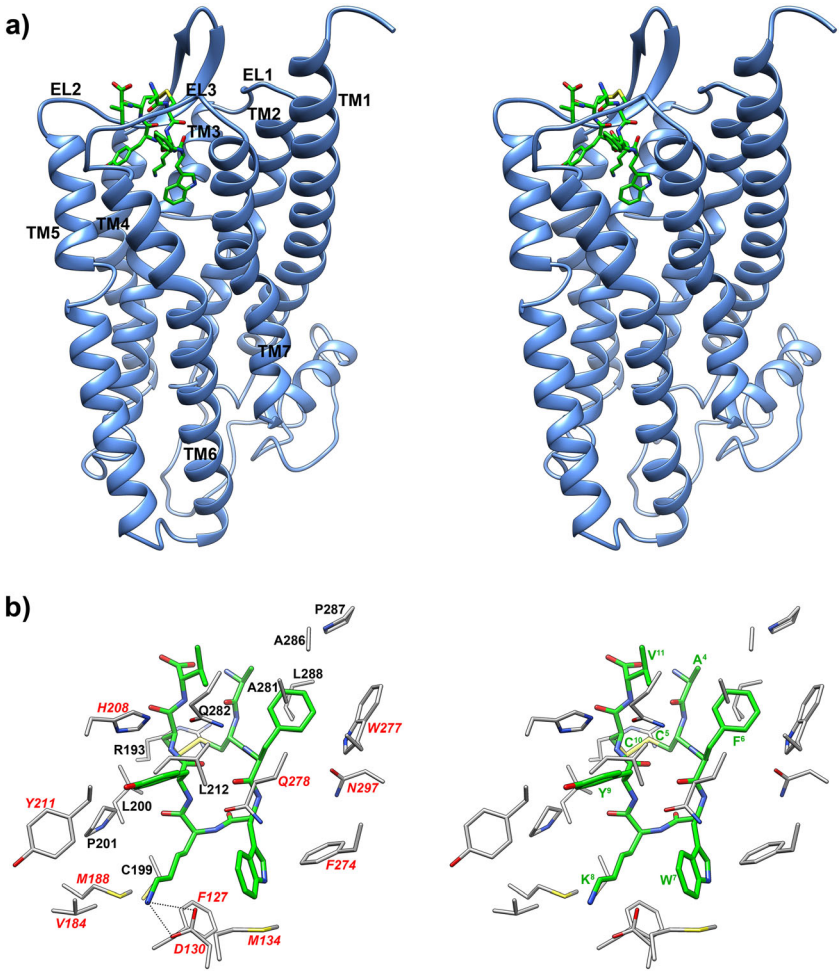

Figure 4. (a) Stereoview of *h*-UTR model complexed with URP. URP heavy atoms are colour coded as in Figure 2. Receptor backbones are represented in azure and labelled. (b) Stereoview of URP within the binding pocket of *h*-UTR. Hydrogen bonds are represented with dashed lines. Labels of UTR residues involved in previous mutagenesis studies are evidenced in red. For the sake of clarity here and throughout the manuscript, the residue numbers of the ligands are reported as apex while those of the receptor are not.

contractile activities supporting the idea that U-II and URP interact with UTR in a distinct manner, i.e. selecting a specific UTR conformation (biased agonism) [18]. Biased agonism would require specific pockets/interactions within UTR, finalized to select distinct UTR conformations that may discriminate U-II and URP biological activities. It was hypothesized that a different conformation of the cyclic portion of the two peptides, β-turn in U-II *versus* γ-turn in URP, would cause the selection of different UTR active states, ultimately triggering a slightly different subset of signalling pathways [16,18]. Hence, we first performed a conformational study on URP by solution NMR. NMR study was performed both in water and in SDS micelle solution. SDS micelles were used because they mimic the cell membrane where UTR is located. A membrane-mediated mechanism of interaction between peptides and their receptors has been postulated [49,50]. According to that mechanism, cell membrane would facilitate peptide increase of local concentration, reduction of rotational and translational freedom, and folding. In fact, several

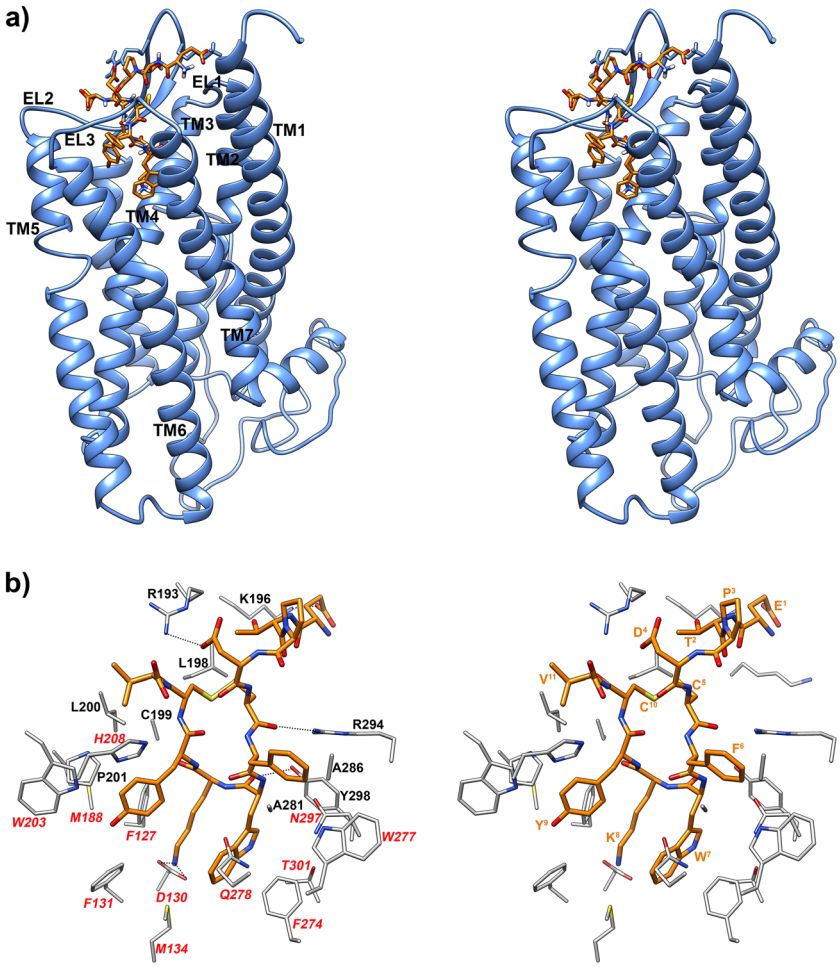

Figure 5. (a) Stereoview of *h*-UTR model complexed with *h*U-II. *h*U-II heavy atoms are colour coded as in Figure 2, apart carbon atoms that are in orange. Receptor backbones are represented in azure and labelled. (b) Stereoview of *h*U-II within the binding pocket of *h*-UTR. Hydrogen bonds are represented with dashed lines. Labels of UTR residues involved in previous mutagenesis studies are evidenced in red.

conformational studies on peptides have been performed in micelle solution [50–54]. Notably, a clear correlation between the conformation in SDS micelles of *h*U-II analogues and their biological activity has been found by us [40,55,56]. NMR-derived structures of URP in SDS solution are shown in Figure 2. Clearly, β-hairpin conformation of the backbone and the side chain cluster of the pharmacophoric residues Trp[7], Lys[8], and Tyr[9], which are distinctive of UTR peptide agonists, are still observable in URP structure. Whereby, URP-obtained NMR structure is very similar to those of other UTR ligands previously found by us and, in particular, to that of *h*U-II (Figure 3). It comes out that divergent actions of URP and *h*U-II cannot derive from different conformation of the ligands as hypothesized by Chatenet *et al.* [18]. That hypothesis was inspired by the comparison of the NMR structure of *h*U-II obtained by us in SDS micelle solution [30] and NMR structure of URP obtained by Chatenet *et al.* in water solution [9]. The last structure is characterized by an inverse γ-turn centred on the Trp-Lys-Tyr sequence as opposite to the β-turn hosted on the corresponding residues of *h*U-II. An inverse γ-turn centred on the Trp-Lys-Tyr is compatible with the data obtained by us in water solution, namely with a NOE contact between H_{α}–NH_{i+2} of Trp[7] and Tyr[9]. However, structure calculations using NMR data from URP spectra acquired in water gave not converging results (data not shown) probably because of a high structural flexibility of the peptide in plain buffer.

In order to determine whether the divergent actions of URP and *h*U-II derive from different interaction with the receptor, NMR-derived structures of URP and *h*U-II were docked within a model of *h*-UTR built by homology using the I-TASSER online server [32–34]. We have already built an *h*-UTR model [39]. It was based on the rhodopsin crystal structure [57]. The current model is based mainly on the *h*-DOR crystal structure [44]. Because the last is a diffusible ligand (peptide) binding GPCR, which share higher sequence homology with *h*-UTR (TM sequence identities: 34.5% to *h*-DOR vs 21.8% to Rho), hence it can be considered a more reliable model than the previous one. In the docking procedures, we hypothesized that peptides bind in the extracellular side of the TM bundle, as observed for all the ligands of class A GPCR [48] and confirmed by mutagenesis studies [58–60]. In this context, only the side chains of residues engaged in orthosteric ligand/GPCR binding in complexes with known crystal structure were considered flexible in the docking procedure. In particular, we took in account *h*-DOR/naltrindole (PDB ID: 4n6h), *m*-MOR/β-funaltrexamine (PDB ID: 4dkl), and NTSR1/neurotensin (PDB ID: 4buo) complexes because they were used as templates by the unbiased homology building procedure of I-TASSER (refer to the preceding texts). A superposition of the putative binding site of *h*-UTR model and *h*-DOR/naltrindole complex is shown in Figure S2 (Supporting Information) as an example.

Journal of PeptideScience

Best poses of complexes of *h*-UTR/URP and *h*-UTR/*h*U-II are shown in Figures 4 and 5, respectively. For both peptides, the predicted binding site is located among TM3/TM7, EL2, and EL3. The β-hairpin is aligned with the receptor helical axis, with the N-termina and C-termina pointing towards the extracellular side. Main interactions between the peptides and UTR are shown in Figure 4b for *h*-UTR/URP and 5b for *h*-UTR/*h*U-II. These findings are in accordance with previous mutagenesis results [58–60]. In fact, many of the receptor residues, involved in the peptides binding in our model, face the binding site pocket of the UT receptor as demonstrated using the substituted-cysteine accessibility method. For some others, the replacement with a cysteine residue caused a complete loss of affinity for the ligands. All these residues are evidenced in Figures 4b–5b. Furthermore, both *h*U-II and URP interact with the ELs but EL1 in accordance with experimental data [61].

Interestingly, comparing our complex model with the peptide-bound GPCR crystal structures solved to date (NTSR1/neurotensin [46] and CXCR4/CVX15 [62]), it can be argued that *h*U-II (and URP, data not shown) binds to the *h*-UTR in a similar fashion as neurotensin to NTSR1 and CVX15 to CXCR4 (Figure S3, Supporting Information).

While the two peptides *h*U-II and URP share similar interactions with the receptor concerning the cyclic region, N-terminal region of *h*U-II establishes large interactions with extracellular loops EL2 of *h*-UTR. In particular, charge-reinforced hydrogen bonds between Glu^1 and Lys196 and between Asp^4 and Arg193 are observable in *h*U-II/*h*-UTR complex (Figure 5). Those interactions cannot be present in URP/*h*-UTR complex. In agreement with our model, dissociation kinetics experiments revealed a putative interaction between UTR and the glutamic residue at position 1 of *h*U-II. Indeed, it was observed that the replacement of this residue by an alanine, i.e. $[Ala^1]$*h*U-II, caused an increase in the dissociation rate of *h*U-II but not URP [18].

Conclusions

We demonstrated that distinct pathophysiological roles for URP and *h*U-II are not related to different conformations of the two peptides, but they likely arise from their different interactions with the UT receptor. Those interactions can stabilize different active conformations of UTR that, in turn, can select specific subset of secondary messengers depending on the ligand-induced adopted conformation.

Acknowledgement

Part of this work was supported by Italian Ministry of Education, University and Research (PRIN 2008, 2008TSWB8K_002; PRIN 2009, 2009EL5WBP_004) and a grant from 'Regione Campania' – Laboratori Pubblici progetto 'Hauteville'.

References

1 Pearson D, Shively JE, Clark BR, Geschwind II, Barkley M, Nishioka RS, Bern HA. Urotensin II: a somatostain-like peptide in the caudal neurosecretory system of fishes. *Proc. Natl. Acad. Sci. U. S. A.* 1980; **77**: 5021–5024.
2 Conlon JM, O'Harte F, Smith DD, Tonon MC, Vaudry H. Isolation and primary structure of urotensin II from the brain of a tetrapod, the frog *Rana ridibunda*. *Biochem. Biophys. Res. Commun.* 1992; **188**: 578–583.
3 Beauvillain JC, Conlon JM, Bern HA, Vaudry H. Cloning of the cDNA encoding the urotensin II precursor in frog and human reveals intense expression of the urotensin II gene in motoneurons of the spinal cord. *Proc. Natl. Acad. Sci. U. S. A.* 1998; **95**: 15803–15808.
4 Coulouarn Y, Jegou S, Tostivint H, Vaudry H, Lihrmann I. Cloning, sequence analysis and tissue distribution of the mouse and rat urotensin II precursors. *FEBS Lett.* 1999; **457**: 28–32.
5 Mori M, Sugo T, Abe M, Shimomura Y, Kurihara M, Kitada C, Kikuchi K, Shintani Y, Kurokawa T, Onda H, Nishimura O, Fujino M. Urotensin II is the endogenous ligand of a G-protein coupled orphan receptor, SENR (GPR14). *Biochem. Biophys. Res. Commun.* 1999; **265**: 123–129.
6 Elshourbagy NA, Douglas SA, Shabon U, Harrison S, Duddy G, Sechler JL, Ao Z, Maleef BE, Naselsky D, Disa J, Aiyar NV. Molecular and pharmacological characterization of genes encoding urotensin II-related peptides and their cognate G-protein coupled receptors from the mouse and monkey. *Br. J. Pharmacol.* 2002; **136**: 9–22.
7 Ames RS, Sarau HM, Chambers JK, Willette RN, Aiyar RV, Romanic AM, Louden CS, Foley JJ, Sauermelch CF, Coatney RW, Ao Z, Disa J, Holmes SD, Stadel JM, Martin JD, Liu WS, Glover GI, Wilson S, McNutty DE, Ellis CE, Eishourbagy NA, Shabon U, Trill JJ, Hay DVP, Ohlstein EH, Bergsma DJ, Douglas SA. Human urotensin-II is a potent vasoconstrictor and agonist for the orphan receptor GPR14. *Nature* 1999; **401**: 282–286.
8 Sugo T, Murakami Y, Shimomura Y, Harada M, Abe M, Ishibashi Y, Kitada C, Miyajima N, Suzuki N, Mori M, Fujino M. Identification of urotensin II-related peptide as the urotensin II immunoreactive molecule in the rat brain. *Biochem. Biophys. Res. Commun.* 2003; **310**: 860–868.
9 Chatenet D, Dubessy C, Leprince J, Boularan C, Carlier L, Segalas-Milazzo I, Guilhaudis L, Oulyadi H, Davoust D, Scalbert E, Pfeiffer B, Renard P, Tonon MC, Lihrmann I, Pacaud P, Vaudry H. Structure-activity relationships and structural conformation of a novel urotensin II-related peptide. *Peptides* 2004; **25**: 1819–1830.
10 Chartrel N, Conlon JM, Collin F, Braun B, Waugh D, Vallarino M, Lahrichi SL, Rivier JE, Vaudry H. Urotensin II in the central nervous system of the frog *Rana ridibunda*: immunohistochemical localization and biochemical characterization. *J. Comput. Neurol.* 1996; **364**: 324–339.
11 Coulouarn Y, Fernex C, Jegou S, Henderson CE, Vaudry H, Lihrmann I Specific expression of the urotensin II gene in sacral motoneurons of developing rat spinal cord. *Mech. Dev.* 2001; **101**: 187–190.
12 Pelletier G, Lihrmann I, Vaudry H. Role of androgens in the regulation of urotensin II precursor mRNA expression in the rat brainstem and spinal cord. *Neuroscience* 2002; **115**: 525–532.
13 Pelletier G, Lihrmann I, Dubessy C, Luu-The V, Vaudry H, Labrie F. Androgenic down-regulation of urotensin II precursor, urotensin II-related peptide precursor and androgen receptor mRNA in the mouse spinal cord. *Neuroscience* 2005; **132**: 689–696.
14 Novellino E, Grieco P, Caraglia M, Budillon A, Franco R, Addeo SR. Peptidic and non peptidic ligands for immunodetection of urotensin-II receptor. PCT Int. Appl. 2008; 21pp. WO 2008095995.
15 Vaudry H, Do Rego JC, Le Mevel JC, Chatenet D, Tostivint H, Fournier A. Urotensin II, from fish to human. *Ann. N.Y. Acad. Sci.* 2010; **1200**: 53–66.
16 Chatenet D, Nguyen TT, Létourneau M, Fournier A. Update on the urotensinergic system: new trends in receptor localization, activation, and drug design. *Front. Endocrinol.* 2013; **3**: 1–13.
17 Maryanoff EB, Kinney AW. Urotensin-II receptor modulators as potential drugs. *J. Med. Chem.* 2010; **53**: 2695–2708.
18 Chatenet D, Létourneau M, Nguyen QT, Doan ND, Dupuis J, Fournier A. Discovery of new antagonists aimed at discriminating UII and URP-mediated biological activities: insight into UII and URP receptor activation. *Br. J. Pharmacol.* 2013; **168**: 807–821.
19 Patel CB, Noor N, Rockman HA. Functional selectivity in adrenergic and angiotensin signaling systems. *Mol. Pharmacol.* 2010; **78**: 983–992.
20 Misika A, Hruby VJ. Optimization of disulfide bond formation. *Pol. J. Chem.* 1994; **68**: 893–899.
21 Hwang TL, Shaka AJ. Water suppression that works. Excitation sculpting using arbitrary wave-forms and pulsed-field gradients. *J. Magn. Res.* 1995; **112**: 275–279.
22 Piantini U, Sorensen OW Ernst RR Multiple quantum filters for elucidating NMR coupling network. *J. Am. Chem. Soc.* 1982; **104**: 6800–6801.
23 Marion D, Wüthrich K. Application of phase sensitive two-dimensional correlated spectroscopy (COSY) for measurements of ^1H-^1H spin-spin coupling constants in proteins. *Biochem. Biophys. Res. Commun.* 1983; **113**: 967–974.
24 Braunschweiler L, Ernst RR. Coherence transfer by isotropic mixing: application to proton correlation spectroscopy. *J. Magn. Reson.* 1983; **53**: 521–528.

25 Jenner J, Meyer BH, Bachman P, Ernst RR. Investigation of exchange processes by two-dimensional NMR spectroscopy. *J. Chem. Phys.* 1979; **71**: 4546–4553.
26 States DJ, Haberkorn RA, Ruben DJ. A two-dimensional nuclear Overhauser experiment with pure absorption phase in four quadrants. *J. Magn. Reson.* 1982; **48**: 286–292.
27 Bartels C, Xia T, Billeter M, Güntert P Wüthrich K The program XEASY for computer-supported NMR spectral analysis of biological macromolecules. *J. Biomol. NMR* 1995; **6**: 1–10.
28 Güntert P, Mumenthaler C Wüthrich K Torsion angle dynamics for NMR structure calculation with the new program DYANA. *J. Mol. Biol.* 1997; **273**: 283–298.
29 Maple J, Dinur U, Hagler AT. Derivation of force fields for molecular mechanics and dynamics from ab initio energy surface. *Proc. Natl. Acad. Sci. U. S. A.* 1988; **85**: 5350–53.
30 Carotenuto A, Grieco P, Campiglia P, Novellino E, Rovero P. Unraveling the active conformation of urotensin II. *J. Med. Chem.* 2004; **47**: 1652–1661.
31 Pettersen EF, Goddard TD, Huang CC, Couch GS, Greenblatt DM, Meng EC, Ferrin TE. UCSF Chimera—a visualization system for exploratory research and analysis. *J. Comput. Chem.* 2004; **25**: 1605–1612.
32 Zhang Y. I-TASSER server for protein 3D structure prediction. *BMC Bioinf* 2008; **9**: 40. DOI: 10.1186/1471-2105-9-40.
33 Kelley LA. Sternberg MJ Protein structure prediction on the Web: a case study using the Phyre server. *Nat. Protoc.* 2009; **4**: 363–371.
34 Roy A, Kucukural A, Zhang Y. I-TASSER: a unified platform for automated protein structure and function prediction. *Nat. Protoc.* 2010; **5**: 725–738.
35 de Vries SJ, van Dijk M Bonvin AMJJ The HADDOCK web server for data-driven biomolecular docking. *Nat. Protoc.* 2010; **5**: 883–897.
36 Wassenaar TA, van Dijk M, Loureiro-Ferreira N, van der Schot G, de Vries SJ, Schmitz C, van der Zwan J, Boelens R, Giachetti A, Ferella L, Rosato A, Bertini I, Herrmann T, Jonker HRA, Bagaria A, Jaravine V, Guntert P, Schwalbe H, Vranken WF, Doreleijers JF, Vriend G, Vuister GW, Franke D, Kikhney A, Svergun DI, Fogh R, Ionides J, Laue ED, Spronk C, Jurka S, Verlato M, Badoer S, Dal Pra S, Mazzucato M, Frizziero E, Bonvin AMJJ. WeNMR: structural biology on the grid. *J. Grid. Comp.* 2012; **10**: 743–767.
37 Kinney WA, Almond HR, Qi J, Smith CE, Santulli RJ, de Garavilla L, Andrade-Gordon P, Cho DS, Everson AM, Feinstein MA, Leung PA, Maryanoff BE. Structure-function analysis of urotensin II and its use in the construction of a ligand-receptor working model. *Angew. Chem. Int. Ed.* 2002; **41**: 2940–2944.
38 Stewart JM, Young JD. *Solid Phase Peptide Synthesis*, Pierce Chemical: Rockford, IL,1984.
39 Grieco P, Carotenuto A, Campiglia P, Gomez-Monterrey I, Auriemma L, Sala M, Marcozzi C, d'Emmanuele di Villa Bianca R, Brancaccio D, Rovero P, Santicioli P, Meini S, Maggi CA, Novellino E. New insight into the binding mode of peptide ligands at urotensin-II receptor: structure-activity relationships study on P5U and urantide. *J. Med. Chem.* 2009; **52**: 3927–3940.
40 Carotenuto A, Auriemma L, Merlino F, Yousif AM, Marasco D, Limatola A, Campiglia P, Gomez-Monterrey I, Santicioli P, Meini S, Maggi CA, Novellino E. Grieco P. Lead optimization of P5U and urantide: discovery of novel potent ligands at the urotensin-II receptor. *J. Med. Chem.* 2014; **57**: 5965–5974.
41 Grieco P, Carotenuto A, Campiglia P, Marinelli L, Lama T, Patacchini R, Santicioli P, Maggi CA, Rovero P, Novellino E. Urotensin-II receptor ligands. From agonist to antagonist activity. *J. Med. Chem.* 2005; **48**: 7290–7297.
42 Wüthrich K. *NMR of Proteins and Nucleic Acids*, John Wiley & Sons, Inc: New York,1986.
43 Wishart DS, Sykes BD, Richards FM. The chemical shift index: a fast method for the assignment of protein secondary structure through NMR spectroscopy. *Biochemistry* 1992; **31**: 1647–1651.
44 Fenalti G, Giguere PM, Katritch V, Huang XP, Thompson AA, Cherezov V, Roth BL, Stevens RC. Molecular control of δ-opioid receptor signalling. *Nature* 2014; **506**: 191–196.
45 Manglik A, Kruse AC, Kobilka TS, Thian FS, Mathiesen JM, Sunahara RK, Pardo L, Weis WI, Kobilka BK, Granier S. Crystal structure of the μ-opioid receptor bound to a morphinan antagonist. *Nature* 2012; **485**: 321–326.
46 Egloff P, Hillenbrand M, Klenk C, Batyuk A, Heine P, Balada S, Schlinkmann KM, Scott DJ, Schuetz M, Plueckthun A. Structure of signaling-competent neurotensin receptor 1 obtained by directed evolutioninEscherichiacoli.*Proc.Natl.Acad.Sci.U.S.A.*2014;**111**:E655–E662.
47 Laskowski RA, Mac Arthur MW, Moss DS, Thornton JM. PROCHECK: a program to check the stereochemical quality of protein structures. *J. Appl. Crystallogr.* 1993; **26**: 283–291.
48 Venkatakrishnan AJ, Deupi X, Lebon G, Tate CG, Schertler GF Babu MM. Molecular signatures of G-protein-coupled receptors. *Nature* 2013; **494**: 185–94.
49 Moroder L, Romano R, Guba W, Mierke DF, Kessler H, Delporte C, Winand J, Christophe J. New evidence for a membrane bound pathway in hormone receptor binding. *Biochemistry* 1993; **32**: 13551–13559.
50 Grieco P, Giusti L, Carotenuto A, Campiglia P, Calderone V, Lama T, Gomez-Monterrey I, Tartaro G, Mazzoni MR, Novellino E. Morphiceptin analogues containing a dipeptide mimetic structure: an investigation on the bioactive topology at the μ-receptor. *J. Med. Chem.* 2005; **48**: 3153–3163.
51 D'Addona D, Carotenuto A, Novellino E, Piccand V, Reubi JC, Di Cianni A, Gori F, Anna Papini AM, Ginanneschi M. Novel sst5-selective somatostatin dicarba-analogues: synthesis and conformation-affinity relationships. *J. Med. Chem.* 2008; **51**: 512–520.
52 Di Cianni A, Carotenuto A, Brancaccio D, Ettore Novellino E, Jean Claude Reubi JC, Karin Beetschen K, Anna Maria Papini AM, Mauro Ginanneschi M. Novel octreotide dicarba-analogues with high affinity and different selectivity for somatostatin receptors. *J. Med. Chem.* 2010; **53**: 6188–6197.
53 Grieco P, Brancaccio D, Novellino E, Hruby VJ, Carotenuto A. Conformational study on cyclic melanocortin ligands and new insight into their binding mode at the MC4 receptor. *Eur. J. Med. Chem.* 2011; **46**: 3721–3733.
54 Mollica A, Carotenuto A, Novellino E, Limatola A, Costante R, Pinnen F, Stefanucci A, Pieretti S, Borsodi A, Samavati R, Zador F, Benyhe S, Davis P, Porreca F, Hruby VJ. Novel cyclic biphalin analogue with improved antinociceptive properties. *ACS Med. Chem. Lett.* 2014; **5**: 1032–1036.
55 Carotenuto A, Auriemma L, Merlino F, Limatola A, Campiglia P, Gomez-Monterrey I, di Villa Bianca R, Brancaccio D, Santicioli P, Meini S, Maggi CA, Novellino E, Grieco P. New insight into the binding mode of peptides at urotensin-II receptor by Trp-constrained analogues of P5U and urantide. *J. Pept. Sci.* 2013; **19**: 293–300.
56 Brancaccio D, Limatola A, Campiglia P, Gomez-Monterrey I, Novellino E, Grieco P, Carotenuto A. Urantide conformation and interaction with the urotensin-II receptor. *Arch. Pharm.* 2014; **347**: 185–192.
57 Palczewski K, Kumasaka T, Hori T, Behnke CA, Motoshima H, Fox BA, Le Trong I, Teller DC, Okada T, Stenkamp RE, Yamamoto M, Miyano M. Crystal structure of rhodopsin: a G protein-coupled receptor. *Science* 2000; **289**: 739–745.
58 Holleran BJ, Domazet I, Beaulieu ME, Yan LP, Guillemette G, Lavigne P, Escher E, Leduc R. Identification of transmembrane domain 6 & 7 residues that contribute to the binding pocket of the urotensin II receptor. *Biochem. Pharmacol.* 2009; **77**: 1374–1382.
59 Sainsily X, Cabana J, Boulais PE, Holleran BJ, Escher E, Lavigne P, Leduc R. Identification of transmembrane domain 3, 4 & 5 residues that contribute to the formation of the ligand-binding pocket of the urotensin-II receptor. *Biochem. Pharmacol.* 2013; **86**: 1584–1593.
60 Sainsily X, Cabana J, Holleran BJ, Escher E, Lavigne P, Leduc R. Identification of transmembrane domain 1 & 2 residues that contribute to the formation of the ligand-binding pocket of the urotensin-II receptor. *Biochem. Pharmacol.* 2014. DOI: 10.1016/j.bcp.2014.08.023.
61 Boivin S, Guilhaudis L, Milazzo I, Oulyadi H, Davoust D, Fournier A. Characterization of urotensin-II receptor structural domains involved in the recognition of U-II, URP, and urantide. *Biochemistry* 2006; **45**: 5993–6002.
62 Wu B, Chien EY, Mol CD, Fenalti G, Liu W, Katritch V, Abagyan R, Brooun A, Wells P, Bi FC, Hamel DJ, Kuhn P, Handel TM, Cherezov V, Stevens RC. Structures of the CXCR4 chemokine GPCR with small-molecule and cyclic peptide antagonists. *Science* 2010; **330**: 1066–1071.

Supporting Information

Additional supporting information may be found in the online version of this article at the publisher's web site.